IEEE Access
Multidisciplinary | Rapid Review | Open Access Journal

Received August 30, 2020, accepted September 17, 2020, date of publication September 21, 2020, date of current version October 1, 2020.

Digital Object Identifier 10.1109/ACCESS.2020.3025570

Fuzzy Active Contour Model Using Fractional-Order Diffusion Based Edge Indicator and Fuzzy Local Fitted Image

HONGLI LV[1,2], FANGJIAN ZHANG[1], AND RENFANG WANG[2]
[1]School of Information Technology, Shangqiu Normal University, Shangqiu 476000, China
[2]College of Big Data and Software Engineering, Zhejiang Wanli University, Ningbo 315100, China

Corresponding author: Renfang Wang (renfang_wang@126.com)

This work was supported in part by the Natural Science Foundation of Zhejiang Province under Grant LY20F020005, in part by the Project of the Science and Technique Plan for Ningbo Municipal under Grant 2019A610108, in part by the Key Scientific Research Projects of Higher Education Institutions of Henan Province under Grant 21A520037, and in part by the Project of the Science and Technology Plan for Zhejiang Province under Grant LGF19F020008.

ABSTRACT Local region-based active contour models (ACMs) can effectively segment images corrupted by intensity inhomogeneity, however, they always converge to local minimum and are sensitive to the initial position of contour. In this paper, a novel fuzzy ACM is proposed to tackle these problems. In order to deal with intensity inhomogeneity, the fuzzy local fitted image is first defined and utilized for constructing a local-region based fuzzy energy term, which is minimized in a variational level set framework to accurately segment inhomogeneous images. Second, the fractional-order diffusion based edge indicator is used to scale the local fuzzy energy term to reduce the effect of intensity inhomogeneity. Third, the fuzzy signed pressure force (FSPF) function defined by local image information is used for constructing the weighted area term to further improve the accuracy of the developed model. Finally, the global FSPF is formulated and used as an adaptive force, which can drive the level set function (LSF) to adaptively move up or down according to image intensity information. Therefore, the initial contour can be initialized as a constant function, which eliminates the problem caused by contour initialization. Moreover, the global FSPF makes the proposed model not easy to fall into local minimum. The results of experiments on synthetic and real images validate the accuracy of the proposed model for inhomogeneous image segmentation.

INDEX TERMS Active contour model, inhomogeneous image segmentation, fuzzy local fitted image, edge indicator, FSPF function.

I. INTRODUCTION

Image segmentation is a primordial task in image analysis and computer vision. The main goal of image segmentation is to partition an image into non-intersected regions with approximately similar property, such as texture, color, intensity, etc [1]. Up to now, many methods have been proposed for image segmentation. Among these methods, ACMs initially proposed by Kass *et al.* [2] have received extensive attention and are widely used for image segmentation. The basic idea of the ACMs is to state the problem of image segmentation as the minimization of an energy functional. Moreover, level set based ACMs implicitly represent an evolving curve as the zero level set of a higher dimension function [3], [4], and the initialized curve is driven by a partial differential equation, which is obtained by minimizing a predefined energy functional. When the evolution of curve stops, the desired boundary of the target object is obtained.

In the past decades, a variety of level set based ACMs, embedding different image features, have been presented for image segmentation. However, the existing ACMs can be roughly dived into three categories: edge-based models [5]–[9], region-based models [10]–[19] and hybrid models [20]–[29]. In edge-based models, an edge indicator defined on image gradient information is used for guiding the evolving curve toward the interest boundary of the target object. These methods generally work well on images with strong boundaries. However, they have difficulty in extracting the weak edge of the target object and are more sensitive to noise, because the effective gradient information near weak edge and noise cannot be obtained.

Generally speaking, region-based models yield better performance on images with weak boundaries, because the curve evolution of these models is urged by a certain region

The associate editor coordinating the review of this manuscript and approving it for publication was Giovanni Pau.

descriptor, which is independent of image gradient information. Specially, one of the typical global region-based models is the Chan-Vese (CV) model [10], which is based on the assumption that image intensities are piecewise constant in the foreground and background. The CV model has some advantages, such as being robust to noise and insensitive to the initial contour. Although global region-based models like the CV model can work well on bimodal images, they usually obtain inaccurate segmentation results in the presence of intensity inhomogeneity. The main reason is because only global image information is incorporated into the defined energy functional.

To address the above problem of global region-based models, local statistical information is considered by researchers to construct local region-based models. By introducing a Gaussian kernel function into the energy functional, Li *et al.* [11], [12] propose the local binary fitting (LBF) model, which uses two local fitting functions to approximate the averages of intensities in a local window inside and outside the contour. In [14], the local entropy weighted region-scalable fitting energy (WRSF) model is proposed to enhance the robust of the LBF model. Zhang *et al.* [13] propose the local image fitting (LIF) model, which minimizes the differences between the original image and the local fitted image defined as the weighted average of two local intensity means. By minimizing the Kullback-Leibler divergence between original image, square image and their corresponding fitted images, Wang *et al.* [15] propose the local hybrid image fitting (LHIF) energy model, which is further improved in [16] by introducing a new inhomogeneity entropy, and they define an entropy weighted fitting (EWF) energy model. In [17], the bias field correction strategy is also used to tackle intensity inhomogeneity. In these models, image intensity is presented as the multiple of the true image and the bias component considered as the inhomogeneity of image. And then, object segmentation and bias component correction are obtained together in a minimization framework. By taking advantages of local image information, the above-mentioned local region-based models can accurately extract the boundary of the target object in the case of intensity inhomogeneity. However, they are heavily dependent on the initial contour. In other words, if the position of the initial contour is inappropriate, the segmentation results of these models may be unsatisfactory.

To deal with the shortcomings of global or local based ACMs and make full use of their advantages, many hybrid ACMs are proposed in the literature. Akram *et al.* [21] propose a local and global fitted image based model, and the Gaussian distribution is used to approximate the bias field. Similar to [29], the coefficient of the weighted area term need to be adjusted according to the position of the initial contour. In [22], global information learned by self-organising maps is used to construct a local energy term. However, if the number of layers is too much, a large computational cost is required. Otherwise, the model cannot effectively segment images with intensity inhomogeneity. In [25], the multiplicative and difference images are used to formulate a new hybrid ACM. However, finding an appropriate method to process the original images is a challenging task. Based on different weighting methods, global and local SPF are used to define hybrid ACMs [26]–[28]. In these hybrid ACMs, local information helps ACMs to accurately segment images with intensity inhomogeneity and global information improves the robustness of ACMs to the initial contour. Therefore, hybrid models always work well on inhomogeneous images.

From the perspective of clustering, region-based ACMs belong to the category of hard one [30]. In contrast, soft clustering methods can retain more information of the original image. The famous fuzzy energy based active contour (FEBAC) [31] is proposed by Stelios Krindis to tackle the problem of local minimum energy. Later on, many fuzzy set based ACMs are presented to enhance the segmentation accuracy of the model. References [32] and [33] use the fuzzy c-means method to initialize the initial contour and the clustering centers, respectively. In [34]–[36], the coefficient constructed by fuzzy method is invoked as the weight to adjust the evolution of level set function. In addition, many fuzzy ACMs [37]–[52] are constructed by using of pseudo LSF, which is identical to the LSF of traditional ACMs. In addition, the energy functional of fuzzy ACMs is often solved by two methods. The first is the Euler-Lagrange equation based gradient descent method [37]–[43]. The second is to directly minimize the difference between the new and old energies [43]–[52].

Specifically, Wu *et al.* [37] put forward an improved fuzzy ACM by introducing kernel metric (KFAC). To segment images having intensity inhomogeneity and slight texture, in [44], the coefficient of variation is used as a regional statistic. Similar to CV, these global fuzzy information based ACMs cannot obtain desirable segmentation results, because only global information of image is used to formulate the fuzzy energy functional. To overcome this problem, many fuzzy ACMs [38], [40], [41], [45], [46], [48], [52] make full use of local fuzzy statistics to cope with intensity inhomogeneity. To improve the robustness of model to initial contour, Sun *et al.* [38] fuse an adaptive contrast constraint into the presented model. By weighting global and local fitting energy, Fang *et al.* [48] present a novel fuzzy region-based ACM, called FRAGL. These models can segmentation inhomogeneous images to some extent. In addition, fuzzy information of the filtered image is also used to define FSPF [53], which guides the movement of the contour. And the optimal membership function is considered as the adjustment weight of each approximated local intensity. Moreover, many convex fuzzy ACMs [42], [44], [45], [48] is designed to prevent the evolution of curve from falling into local minimum.

As mentioned above, fusing local image information into the defined energy functional is an effective way to cope with intensity inhomogeneity. In this paper, we present a novel fuzzy energy-based ACM. First of all, the fuzzy local fitted image (FLFI) is defined as the weighted average of local fuzzy means on the two sides of the evolving curve,

and the local-region based fuzzy energy term is defined as the Kullback-Leibler divergence between the original image and FLFI. Secondly, the fractional-order based diffusion method is utilized to smooth the original image, and the edge indicator is constructed on the filtered image. In order to improve the ability of the model to segment inhomogeneous images, the previously defined local fuzzy energy term is scaled by the edge indicator. And then, we respectively formulate local and global FSPF. The first one is considered as the weight of the area term, and the other one is taken as an adaptive force. Because their signs are opposite inside and outside the object, the weighted area term can automatically drive the evolving curve toward the desired object boundaries. Meanwhile, the adaptive force can drive the LSF to automatically increase or decrease according to image intensity information, which allows the initial contour of the proposed model to be initialized as a constant function. Therefore the problem caused by contour initialization can be eliminated. The experimental results demonstrate that the proposed method is able to segment the images with intensity inhomogeneity in terms of efficiency and accuracy.

In summary, the main contributions of the paper are listed as follows:

1) The fractional-order diffusion based edge indicator and FLFI are constructed to reduce the effect of intensity inhomogeneity in the given images.
2) The area term weighted by the defined local FSPF is proposed to enhance the ability of our model to segment inhomogeneous images. Moreover, local FSPF can control the direction of the evolving curve, which makes the initial contour automatically move toward the desired object boundaries.
3) The adaptive force based on the formulated global FSPF is used to cope with the position problem of the initial contour. And the evolution of the level set of the proposed model can start with a constant function without considering the position of the initial contour.

The rest of the paper is organized as follows. Section 2 briefly introduces some related work and discusses their limitations to prepare the description of the proposed model, which will be described in detail in Section 3. Section 4 presents the experimental results. Finally, conclusions are drawn in Section 5.

II. RELATED WORK

ACMs have become one of the most popular methods for image segmentation due to easily handling the topological changes of evolving curve. In this section, we will give a brief review on related work and indicate their limitations.

A. CV MODEL

Let $I : \Omega \to R$ be an input gray level image in domain Ω. A closed curve C is implicitly represented by the zero level set of the LSF $\phi(x)$. Variable x is a point in domain Ω with intensity $I(x)$. The purpose of the CV model [10] is to look for a optimal partition by minimizing the following energy functional:

$$\begin{aligned} E^{CV}(\phi(x), c_1, c_2) = \mu \cdot \int_\Omega \delta_\varepsilon(\phi(x))|\nabla\phi(x)|dx \\ + \lambda_1 \int_\Omega |I(x) - c_1|^2 M_1(\phi(x))dx \\ + \lambda_2 \int_\Omega |I(x) - c_2|^2 M_2(\phi(x))dx \end{aligned} \quad (1)$$

where $M_1(\phi(x)) = H_\varepsilon(\phi(x))$ and $M_2(\phi(x)) = 1 - H_\varepsilon(\phi(x))$, ∇ is gradient operator, and $H_\varepsilon(\cdot)$ is the regularized Heaviside function formulated as:

$$H_\varepsilon(z) = \frac{1}{2}\left(1 + \frac{2}{\pi}\arctan\left(\frac{z}{\varepsilon}\right)\right), \quad z \in \mathbb{R}. \quad (2)$$

Dirac function $\delta_\varepsilon(z)$ is the derivative of $H_\varepsilon(z)$, and ε is a small positive constant. λ_1, λ_2 and μ are fixed positive parameters. c_1 and c_2 are two constants that denote the average intensities inside and outside the contour C, respectively. The LSF $\phi(x)$ is expressed by:

$$\begin{cases} C = \{x \in \Omega : \phi(x) = 0\} \\ inside(C) = \{x \in \Omega : \phi(x) > 0\} \\ outside(C) = \{x \in \Omega : \phi(x) < 0\} \end{cases} \quad (3)$$

By minimizing the energy functional (1) with regard to c_i, $i = 1, 2$, the following equations can be obtained:

$$c_i = \frac{\int_\Omega I(x)M_i(\phi(x))dx}{\int_\Omega M_i(\phi(x))dx}, \quad i = 1, 2 \quad (4)$$

Obviously, c_1 and c_2 respectively represent the global statistical information inside and outside the contour C. Therefore, if the intensity of image is inhomogeneous, they may be far different from the actual data. As a result, the CV model usually fails to segment images corrupted by intensity inhomogeneity. However, the CV model is less sensitive to initial contour and not easy to trap into local minimum.

B. LBF MODEL

To segment images with intensity inhomogeneity, the LBF model [11], [12] is proposed by introducing a Gaussian kernel function. The energy functional of the LBF model is expressed by:

$$\begin{aligned} &E^{LBF}(\phi(x), f_1(x), f_2(x)) \\ &= \lambda_1 \int_\Omega \left[\int_\Omega K_\sigma(x - y)|I(y) - f_1(x)|^2 M_1(\phi(y))dy\right] dx \\ &\quad + \lambda_2 \int_\Omega \left[\int_\Omega K_\sigma(x - y)|I(y) - f_2(x)|^2 M_2(\phi(y))dy\right] dx \end{aligned} \quad (5)$$

where λ_1 and λ_2 are positive constants. K_σ is the Gaussian kernel function with standard deviation σ. Two smooth functions $f_1(x)$ and $f_2(x)$ are used to approximate the local averages of intensities inside and outside the contour in a local window.

Keeping LSF $\phi(x)$ fixed and minimizing the energy functional (5), $f_1(x)$ and $f_2(x)$ can be obtained:

$$f_i(x) = \frac{\int_\Omega K_\sigma(x-y)I(y)M_i(\phi(y))dy}{\int_\Omega K_\sigma(x-y)M_i(\phi(y))dy}, \quad i = 1, 2 \tag{6}$$

Different from c_1 and c_2 in the CV model, $f_1(x)$ and $f_2(x)$ are local averages of the input image intensities in a local window. Therefore, the LBF model can effectively segment images with intensity inhomogeneity. However, the LBF model is easy to trap into local minimum and sensitive to the position of the initial contour.

C. LIF MODEL

The LIF model [13] assumes that the local region N_x is piecewise smooth, and the center intensity of N_x can be fitted by the local intensity averages. The energy functional of the LIF model aims to minimize the differences between the original image and the local fitted image, which is formulated as follows:

$$E^{LIF}(\phi(x)) = \frac{1}{2}\int_\Omega |I(x) - I^{LFI}(x)|^2 dx \tag{7}$$

where $I^{LFI}(x)$ is the local fitted image, which is expressed as:

$$I^{LFI}(x) = M_1(\phi(x))f_1(x) + M_2(\phi(x))f_2(x) \tag{8}$$

here $f_1(x)$ and $f_2(x)$ represent the local intensity averages inside and outside the contour in the local region N_x.

Segmentation results of the LIF model are similar to that of the LBF model. But compared with the LBF model, the LIF model needs less computational time, because the Gaussian filtering process is used to smooth the level set function. Moreover, the LIF model still suffers from the problem of the position of the initial contour, that is, whether the selected position of the initial contour is appropriate is an important factor affecting the accuracy of the segmentation results.

D. FEBAC MODEL

The basic assumption of the FEBAC model [31] is similar to that of the CV model. That is, the image intensities in the foreground and background are piecewise constant. By introducing the membership value $u(x)$, the FEBAC model first defines a pseudo LSF, which is given by:

$$\begin{cases} C = \{x \in \Omega : u(x) = 0.5\} \\ inside(C) = \{x \in \Omega : u(x) > 0.5\} \\ outside(C) = \{x \in \Omega : u(x) < 0.5\} \end{cases} \tag{9}$$

And then the fuzzy energy functionanl of the FEBAC model is expressed as:

$$E^{FEBAC}(u, c_1, c_2) = \lambda_1 \int_\Omega [u_1(x)]^m |I(x) - c_1|^2 dx + \lambda_2 \int_\Omega [u_2(x)]^m |I(x) - c_2|^2 dx \tag{10}$$

where λ_1 and λ_2 are positive constants. $u_1(x) = u(x) \in [0, 1]$ and $u_2(x) = 1 - u(x)$ indicate the degree of the membership of intensity $I(x)$ belong to c_1 and c_2, respectively. The weighting exponent $m(m > 1)$ is usually set to 2.

Keeping $u(x)$ fixed and minimizing the energy functional (10) with respect to c_1 and c_2, the following equations used to update c_1 and c_2 can be obtained:

$$c_i = \frac{\int_\Omega [u_i(x)]^m I(x) dx}{\int_\Omega [u_i(x)]^m dx}, i = 1, 2 \tag{11}$$

Similar to the CV model, when the basic assumption that image intensities are piecewise constant in each region (foreground or background) is not met, FEBAC model usually cannot extract the desirable boundaries of the target objects.

III. THE PROPOSED MODEL

As mentioned in Section 2, global-based ACMs lack the ability to segment images with intensity inhomogeneity. In contrast, the local-based ACMs can obtain more accurate segmentation results, however, these local-based ACMs are more sensitive to the position of the initial contour. To cope with these problems, in this section, we present an adaptive fuzzy energy based ACM and describe it in detail. We firstly present the fractional-order based diffusion filter, and define an edge indicator. Then, we formulate the global and local FSPF, and prove that their signs are opposite inside and outside the object. Finally, we define a novel fuzzy energy functional and give the algorithm steps.

A. FRACTIONAL-ORDER DIFFUSION BASED EDGE INDICATOR

Inspired by [54]–[56], in this subsection, we aim to extract the underlying object edge where the initial contour needs to stop. For this purpose, the fractional-order derivative based Perona-Malik diffusion is used to smooth the original image. This diffusion process can yield a piecewise constant results while preserving edges and suppressing staircase [55], [56]. Specially, the input image is first smoothed by the following fractional-order diffusion equation:

$$\frac{\partial I}{\partial t} = -D_x^{\alpha *}\left(g(DC)D_x^\alpha I\right) - D_y^{\alpha *}\left(g(DC)D_y^\alpha I\right) \tag{12}$$

where $D_x^{\alpha *}$ and $D_y^{\alpha *}$ are the conjugates of fractional-order derivatives D_x^α and D_y^α, $\alpha \in (1, 2)$. $g(DC) = exp(-DC/100)$ is diffusivity function, and DC stands for difference curvature, which is expressed as:

$$DC = ||I_{\eta\eta}| - |I_{\xi\xi}|| \tag{13}$$

and

$$I_{\eta\eta} = \frac{I_x^2 I_{xx} + 2I_x I_y I_{xy} + I_y^2 I_{yy}}{I_x^2 + I_y^2} \tag{14}$$

$$I_{\xi\xi} = \frac{I_y^2 I_{xx} - 2I_x I_y I_{xy} + I_x^2 I_{yy}}{I_x^2 + I_y^2} \tag{15}$$

where I_x and I_y represent the first-order derivatives, I_{xx} and I_{yy} denote the second-order derivatives. The partial differential equation defined in (12) can be solved iteratively in the frequency-domain, for details refer to [55], [56].

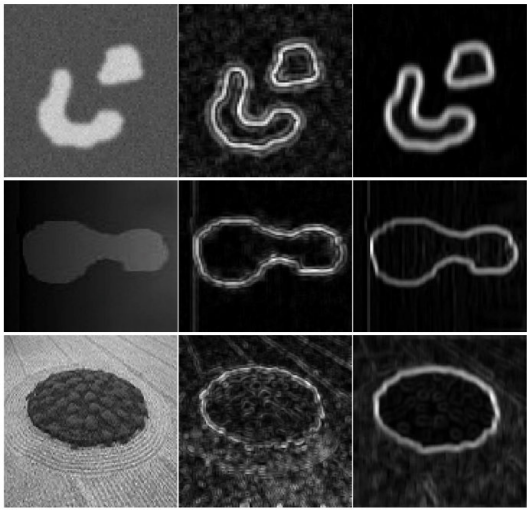

FIGURE 1. (a) Original images. (b) Results of LoG filtering followed by zero-crossing based on the diffused images. (c) Results of the proposed edge indicator.

As pointed out in [57], the value of DC is large at the object edges, while it is small in flat regions. Therefore, the diffusion process conducted by (12) can efficiently smooth the flat regions while preserving important image edges, which are related to the boundaries of the target object. Let $I^k(s)$ be the result of the k iterations, the adaptive order-based edge indicator of the smoothed image $I^k(s)$ is defined as follows:

$$M^k(s) = \frac{1}{25}\sum_{t\in N_s}\frac{\left|\left(I^k(t)\right)^{\beta(s)} - (m(s))^{\beta(s)}\right|}{m(s)} \tag{16}$$

where $m(s)$ is the sample mean of the local rectangular window N_s of size 5×5, and adaptive order function $\beta(s)$ is defined by:

$$\beta(s) = \frac{2 * (1+T)}{1+\sqrt{I_x^2(s)+I_y^2(s)}} \tag{17}$$

here T is the maximum value of $\sqrt{I_x^2(s)+I_y^2(s)}(s \in \Omega)$, and I is the normalized result of the smoothed image $I^k(s)$. It is worth noting that when the condition $mean(|M^k(s) - M^{k-1}(s)|) < 0.1$ is met, iteration process conducted by (12) is terminated. As shown in Fig. 1, The proposed edge indicator can provide more reliable results compared to the traditional edge indicator (e.g. Laplacian of Gaussian (LoG) filter).

B. LOCAL FUZZY ENERGY TERM

Local image information plays an important role in dealing with intensity inhomogeneity. Therefore, we consider making full use of fuzzy local information to construct the proposed local energy term. We first defined the fuzzy local fitted image as follows:

$$I^{FLFI}(x) = u_1(x)m_1(x) + u_2(x)m_2(x) \tag{18}$$

where $m_1(x)$ and $m_2(x)$ are local fuzzy clustering center functions and defined by

$$m_i(x) = \frac{\int_\Omega K_\sigma(x-y)I(y)[u_i(y)]^m dy}{\int_\Omega K_\sigma(x-y)[u_i(y)]^m dy}, \quad i = 1, 2 \tag{19}$$

Obviously, $m_1(x)$ and $m_2(x)$ calculate the local intensity means inside and outside the contour C in a neighbourhood of x. I^{FLFI} can be considered as the fuzzy approximation of the original image I in a local window.

To take advantage of the defined FLFI, in this paper, Kullback-Leibler divergence is used to quantify the differences between the original image I and its approximation FLFI, and the edge indicator scaled local fuzzy energy term is defined by:

$$E^L(u(x)) = \int_\Omega \left[I(x)log\left(\frac{I(x)}{I^{FLFI}(x)}\right) + I^{FLFI}(x)log\left(\frac{I^{FLFI}(x)}{I(x)}\right)\right] W(x)dx \tag{20}$$

where $W(x) = 1/(1 + exp(-M(x))$ is used to scale the Kullback-Leibler divergence between I and I^{FLFI}. $M(x)$ is the normalized form of the edge indicator defined in (16), which is obtained when the iteration process conducted by (12) is terminated.

C. GLOBAL AND LOCAL FSPF

In our works [41], a global FSPF is defined as:

$$spf(I(x)) = \frac{I(x) - (0.5c_1 + 0.5c_2)}{max\left(|I(x) - (0.5c_1 + 0.5c_2)|\right)} \tag{21}$$

where c_1 and c_2 are defined in (11). It has been proved that $spf(I(x))$ has values in the range $[-1, 1]$. Although it can efficiently modulate the signs of the pressure forces inside and outside the region of interest, the constant weights (e.g., 0.5) cannot carry more information of the images.

To overcome this drawback, in this subsection, we propose two novel FSPF. Let $spf_G(I(x))$ and $spf_L(I(x))$ be global FSPF and local FSPF, respectively, then they are defined by:

$$spf_G(I(x)) = \frac{I(x) - (u_1(x)c_1 + u_2(x)c_2)}{max\left(|I(x) - (u_1(x)c_1 + u_2(x)c_2)|\right)} \tag{22}$$

$$spf_L(I(x)) = \frac{I(x) - (u_1(x)m_1(x) + u_2(x)m_2(x))}{max\left(|I(x) - (u_1(x)m_1(x) + u_2(x)m_2(x))|\right)} \tag{23}$$

where c_1, c_2 are defined in (11) and $m_x(x), m_2(x)$ are defined in (19). From the definition, we can see that $spf_G(I(x))$ is a global measure which contains the global statistical information, and $spf_L(I(x))$ is a local measure which contains the local statistical information. The FSPF functions defined in (22) and (23) also have values in range $[-1, 1]$. For simplicity, we prove this property only for a binary image. Let $\Omega\backslash\omega$ and ω be the background and the object, respectively, then a binary image can be expressed as:

$$I(x,y) = \begin{cases} a, & (x,y) \in \omega \\ b, & (x,y) \in \Omega\backslash\omega, \end{cases} \tag{24}$$

where $a, b > 0$ with $a \neq b$.

Theorem 1: Let I be a binary image defined by (24). Then one has

$$sign\left(spf_G(I(x))\right) = \begin{cases} +sign(a-b), & in\ \omega \\ -sign(a-b), & in\ \Omega \setminus \omega. \end{cases} \tag{25}$$

Proof: see Appendix A.

Theorem 2: Let I be a binary image defined by (24). Then one has

$$sign\left(spf_L(I(x))\right) = \begin{cases} +sign(a-b), & in\ \omega \\ -sign(a-b), & in\ \Omega \setminus \omega. \end{cases} \tag{26}$$

Proof: see Appendix B.

Compared with the FSPF proposed in [53], the proposed FSPF has the following differences:

1) On one hand, c_1 and c_2 of the proposed $spf_G(I(x))$ denote the fuzzy average intensities inside and outside the contour C, respectively. On the other hand, the weights of c_1 and c_2 are not constant (eg. 0.5), but membership values. Therefore, the designed $spf_G(I(x))$ can retain more information of the original image.
2) The $spf_G(I(x))$ is designed to reduce the dependence of ACMs on initial contour, not to control the direction of the evolving curve, which is why the level set of the proposed model can start with a constant function.
3) The purpose of $spf_L(I(x))$ defined in (23) is the same as that of the FSPF proposed in [53], which is to control the direction of the evolving curve. However, the $spf_L(I(x))$ is defined by the membership value weighted local mean, which enables the direction of the evolving curve make adjustments automatically based on local information.

D. EVOLUTION EQUATION OF THE PROPOSED MODEL

The fuzzy energy functional of the proposed model is expressed as:

$$E(u(x), m_1(x), c_1, c_2) = \lambda E^L(u(x)) + \mu L(u(x)) + \nu A(u(x)) + \gamma spf_G(I(x)) \tag{27}$$

where λ, μ, ν and γ are positive constants. $u(x)$ is pseudo LSF defined in (9). $L(u(x))$ and $A(u(x))$ are defined by:

$$L(u(x)) = \int_\Omega \delta_\varepsilon(u(x) - 0.5)|\nabla(u(x) - 0.5)|dx \tag{28}$$

and

$$A(u(x)) = \int_\Omega spf_L(I(x))H_\varepsilon(u(x) - 0.5)dx \tag{29}$$

where $\delta_\varepsilon(z)$ is the derivative of the regularized Heaviside function $H_\varepsilon(z)$ defined in (2). The energy functional $L(u(x))$ is length term, which is used to smooth the pseudo zero level contour. $A(u(x))$ computes the weighted area of the region $\{x \in \Omega : u(x) > 0.5\}$. Since signs of $spf_L(I(x))$ are opposite inside and outside the object, the pseudo zero level contour can automatically shrink or expand. And the global FSPF $spf_G(I(x))$ can be seen as an adaptive force, which drives the pseudo LSF to automatically increase or decrease according to image intensity information.

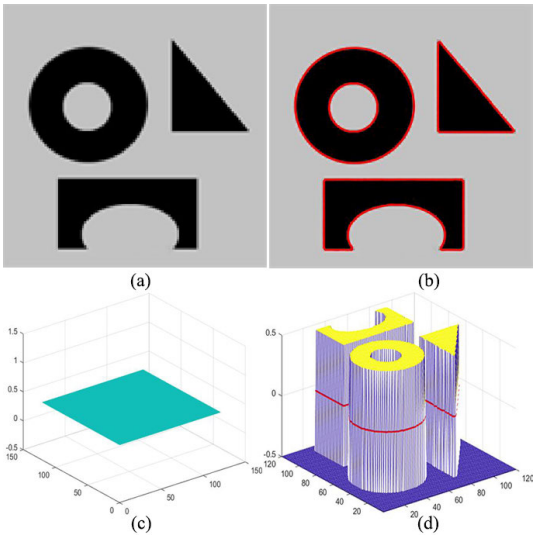

FIGURE 2. Contribution of $spf_G(I(x))$. (a) Original image. (b) Segmentation result. (c) 3D plot of the initial constant pseudo LSF. (d) 3D plot of the final pseudo LSF.

Keep $m_i(x)(i = 1, 2)$ and $c_i(i = 1, 2)$ fixed, we minimize the fuzzy energy functional (27) with respect to $u(x)$. The following formulation is obtained to update the pseudo level set $u(x)$:

$$\frac{\partial u}{\partial t} = \lambda e(x) + \mu\delta_\varepsilon(u(x) - 0.5)div\left(\frac{\nabla(u(x) - 0.5)}{|\nabla(u(x) - 0.5)|}\right) + \nu spf_L(I(x))\delta_\varepsilon(u(x) - 0.5) + \gamma spf_G(I(x)) \tag{30}$$

and

$$e(x) = (m_1(x) - m_2(x))\left(\frac{I(x)}{I^{FLFI}(x)} - 1 - log\frac{I^{FLFI}(x)}{I(x)}\right)W(x) \tag{31}$$

where $div(\cdot)$ is the divergence operator.

Next, we analyse the characteristic of the global FSPF $spf_G(I(x))$ based on the following equation:

$$\frac{\partial u}{\partial t} = spf_G(I(x)) \tag{32}$$

From the **Theorem 1**, It can be seen that the $spf_G(u(x))$ has opposite signs inside and outside the object. If $spf_G(u(x)) > 0$, then $\partial u/\partial t > 0$, and (32) makes u increase; Conversely, if $spf_G(u(x)) < 0$, then $\partial u/\partial t < 0$, and (32) makes u decrease. This characteristic can drive the pseudo LSF u to move up or down according to the image intensity information. Therefore, a constant function can be used as the initialization of $u(x)$. Taking a binary image (Fig. 2a) as an example, the initial contour is set to be a constant function (e.g., $u(x) = 0.5, x \in \Omega$) shown in Fig. 2c. The segmentation result of the proposed model is shown in Fig. 2b, and Fig. 2d shows the 3D plot of the final pseudo LSF, and the contour $C = \{x \in \Omega : u(x) = 0.5\}$ is marked by red line. This example demonstrates that the proposed model is less troubled by the problem of the initial contour.

It is worth noting that the proposed model is different from the hybrid ACMs proposed in [27], [48]. In one hand, the gradient information of LSF used in [27] is sensitive to the edge of object, which cannot effectively deal with weak boundaries. On the other hand, the global SPF proposed in [27] and the proposed model are used to enhance the robustness of the models to initial contour. However, the proposed global SPF constructed by fuzzy image information can makes the level set evolution start with a constant function. In addition, the hybrid averages in FRAGL [48] based on global and local intensity ones may not fit the local information, because the global averages will be far different from the actual data the intensity of image is inhomogeneous. Therefore, FRAGL cannot deal with images with serious intensity inhomogeneity. However, in the proposed model, Kullback-Leibler divergence based local term is used to effectively capture the local information, and local FSPF can automatically adjust the direction of the evolving curve in a local manner. They make the proposed more robustness to intensity inhomogeneity.

E. ALGORITHM

In this subsection, a finite difference scheme is used to numerically solve the proposed model. The iterative formula of (30) can be simply written as:

$$u^{k+1} = u^k + \Delta t \cdot A(u^k) \tag{33}$$

where Δt is the time step, u^k is the result of the kth iteration, and $A(u^k)$ is the approximation of the right hand side of (30). In order to obtain a stable updating of u, the input image is first normalized by the following equation:

$$I = \frac{I - I_{min}}{I_{max} - I_{min}} \tag{34}$$

where I_{min} and I_{max} represent the minimum and maximum of image intensity. Note that u may break the constraint $(0 \le u \le 1)$ during the evolution. Therefore, u is reset at the end of each iteration according to the following approach:

$$u = \begin{cases} 0, & if\ u < 0 \\ u, & if\ 0 \le u \le 1 \\ 1, & if\ u > 1 \end{cases} \tag{35}$$

And the result of each iteration is smoothed by the Gaussian filtering method, which is expressed as:

$$u^{k+1} = K_\rho u^k \tag{36}$$

where K_ρ is the Gaussian kernel function with standard deviation ρ. For simplicity, in this paper, the parameter ρ is set to 0.55 for all experiments.

In summary, the main procedures of the proposed algorithm are given as follows:

1: *Normalize the input image by (34).*
2: *Initialize the pseudo LSF u to be a constant function or a step function defined in (9).*
3: *Compute c_i and m_i $(i = 1, 2)$ according to (11) and (19).*
4: *Update u according to (33), and then normalize it by (35).*
5: *Smooth u by (36).*
6: *Check whether the evolution is stationary. If not, return to step 2.*

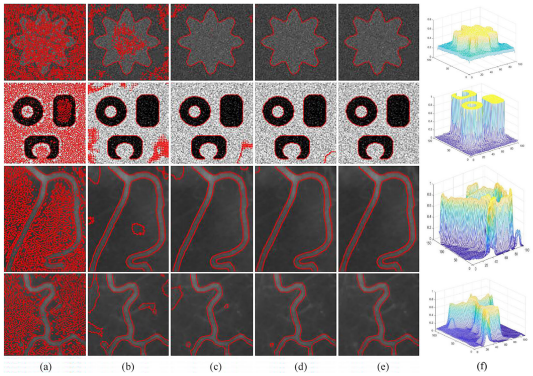

FIGURE 3. Effectiveness of the initial constant function. (a)-(d) Segmentation results of the proposed model after 2, 30, 100, 200 iterations. (e) Final results of the proposed model. (f) 3D plots of the final pseudo LSF.

IV. EXPERIMENTAL RESULTS

In this section, the proposed model will be tested on synthetic and real images. All experiments are conducted in Matlab (R2019b) programming environment on Intel(R) Core(TM) i7-4720HQ CPU 2.6GHz and RAM 16.0GB. Unless otherwise specified, the parameters are set by default as follows: $\lambda = \nu = 1$, $\gamma = 0.05$, $\mu = 0.5$, $\Delta t = 0.05$ and $\alpha = 1.5$. To validate the effectiveness of the developed model, we compare the developed model with CV [10], LBF [12], LIF [13], EWF [16], FEBAC [21], FRAGL [48] and GLSEPF [28] to display their performance differences. The parameters of the compared methods are set according to the original papers.

A. EFFECTIVENESS OF THE PROPOSED MODEL

In this subsection, we first validate the effectiveness of the proposed model on four images, and the initial contour is set to be a constant function (e.g., $u(x) = 0.5, x \in \Omega$). Figs. 3(a)-(d) show the intermediate results of the proposed model after 2, 30, 100, 200 iterations. The final segmentation results marked by red line are shown in Fig. 3(e), and the 3D plot of the final pseudo LSF are shown in Fig. 3(f). It can be observed that the developed model can obtain desirable segmentation results for these images, whether it is noisy images or images with intensity inhomogeneity. This experiment demonstrates that the defined global FSPF $spf_G(I(x))$ can drive the pseudo level set function $u(x)$ to automatically move up or down, which allows $u(x)$ to be initialized as a constant function. Therefore, the problem caused by the position of the initial contour can be alleviated to some extent. In addition, the corresponding fuzzy local fitted images are shown in row 1 of Fig. 4, which demonstrate that a large number of the undesired background information of the original images is greatly suppressed. Moreover, these fitted images I^{FLFI} highlight the importance of the desirable objects and reduce the adverse effects of the complex

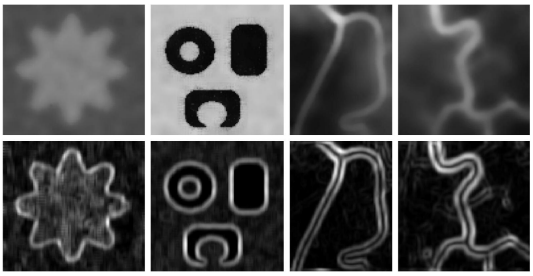

FIGURE 4. Effectiveness of the proposed FLFI and edge indicator. Row 1: Fuzzy local fitted images I^{FLFI}. Row 2: Edge indicator $M(x)$.

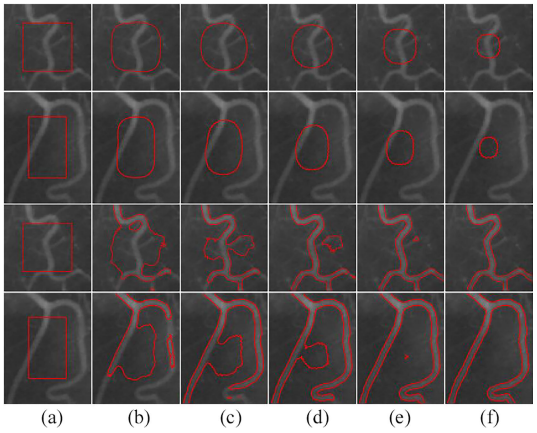

FIGURE 5. Contribution of $spf_L(I(x))$. (a)Original images with initial contour. (b)-(f): Results after 50, 100, 150, 200, 250 iterations. Rows 1 and 2: local FSPF is replaced by the constant 1. Rows 3 and 4: local FSPF is reserved.

background in image segmentation of the developed model. Row 2 of Fig. 4 shows the corresponding edge indicators, which provide the underlying boundaries of the target objects and efficiently suppress the complex texture components. Therefore, the proposed edge indicator weighting method can hance the model's ability to segment images with intensity inhomogeneity.

To demonstrate the contribution of the proposed local FSPF $spf_L(I(x))$, we conduct the following experiment shown in Fig. 5, and the initial contours are set as a step function according to the (9). Fig. 5(a) shows the original images with initial contour. Figs. 5(b)-(f) show evolution results after 50, 100, 150, 200, 250 iterations, respectively. Rows 1 and 2 are the evolution process of the curve by setting $spf_L(I(x))$ to 1. We can discover that the contours are gradually contracted, if fact, the contours will disappear after 300 iterations. When $spf_L(I(x))$ is reserved, the proposed model can obtain desirable segmentation results. The main reason is that the proposed local FSPF can efficiently modulate the direction of the evolution of the curve.

B. COMPARISONS WITH THE EXISTING SEGMENTATION ALGORITHMS

1) ROBUSTNESS TO INITIAL CONTOUR

To demonstrate the robustness of the developed method to initial contour, the following experiments are conducted on

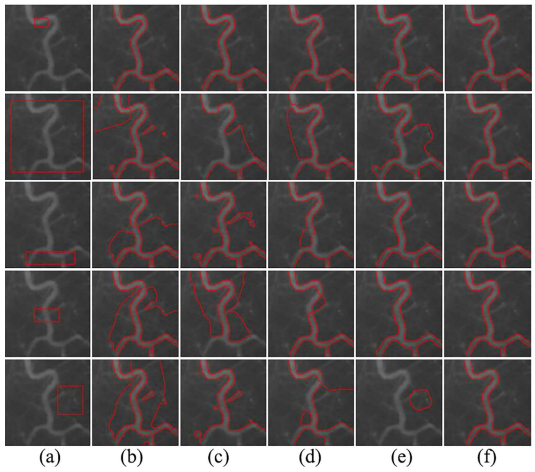

FIGURE 6. Segmentation results of vessel image with different initial contours. (a) Original image with initial contour. (b)-(f) Results of LBF, LIF, EWF, GLSEPF and our model, respectively.

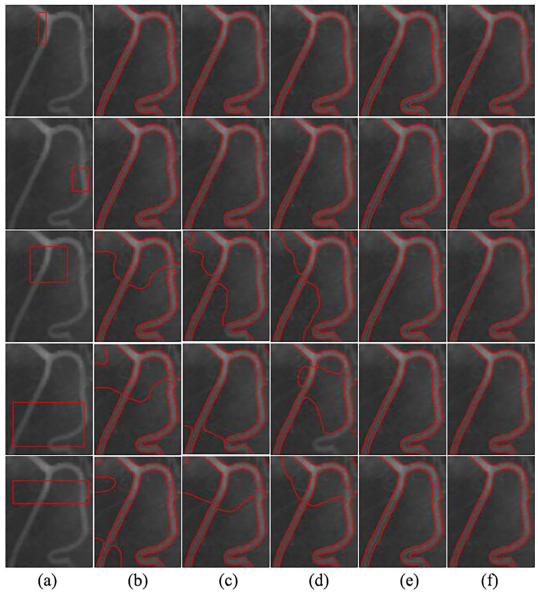

FIGURE 7. Segmentation results of vessel image with different initial contours. (a) Original image with initial contour. (b)-(f) Results of LBF, LIF, EWF, GLSEPF and our model, respectively.

two vessel images with intensity inhomogeneity. Given that CV, FEBAC and FRAGL cannot efficiently segment images with intensity inhomogeneity, which will be shown in the subsequent experiments, we just compare the developed model with LBF, LIF, EWF and GLSEPF. The segmentation results of the related models are shown in Figs. 6 and 7. In Fig. 6, LBF, LIF and EWF only get the desirable segmentation results in the row 1. GLSEPF falls into local minimum in rows 2 and 5. Fig. 7 shows that LBF, LIF and EWF can correctly segment the input image in rows 1 and 2, and their performance in other situation are worse. It is also can be seen that the developed model and GLSEPF work well on the second image with all initial contours. From experiments in Figs. 6 and 7, we can get the following conclusions to a certain extent. On one hand, the traditional local information

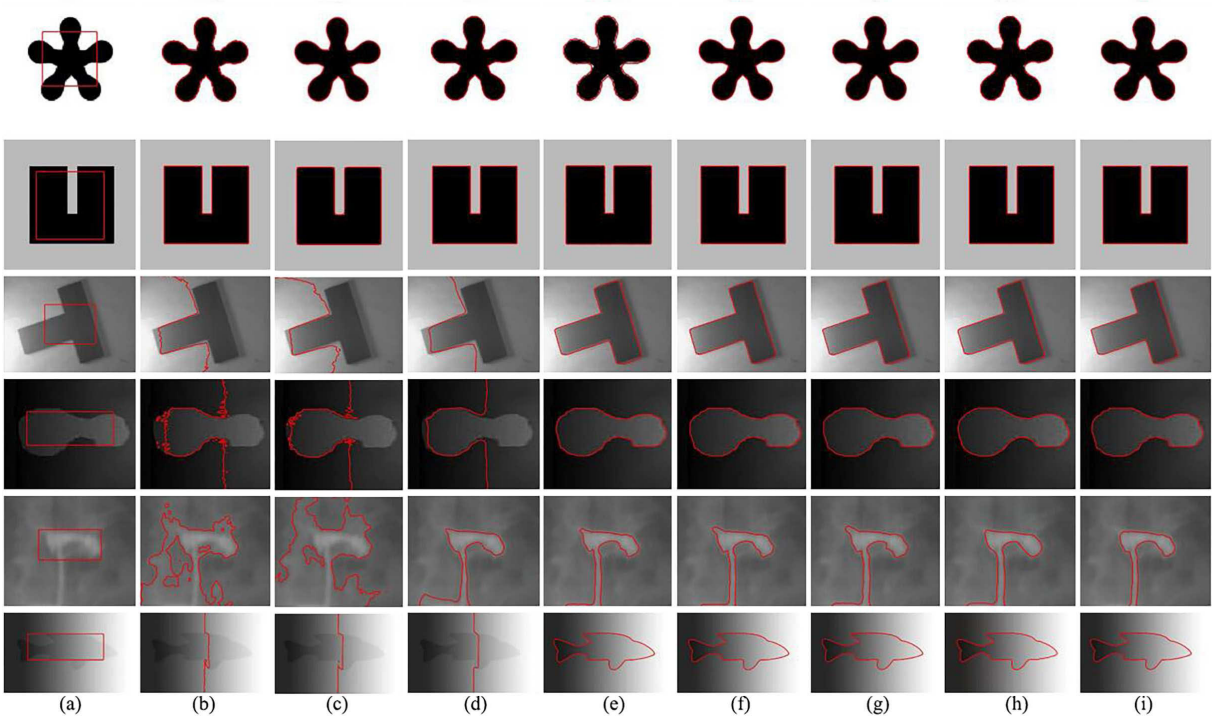

FIGURE 8. Segmentation results of bimodal and inhomogeneous images. (a) Original images with initial contours. (b)-(i) Results of CV, FEBAC, FRAGL, EWF, LBF, LIF, GLSEPF and our model. Rows 1 and 2: results of two homogeneous images. Rows 3-6: results of four inhomogeneous images.

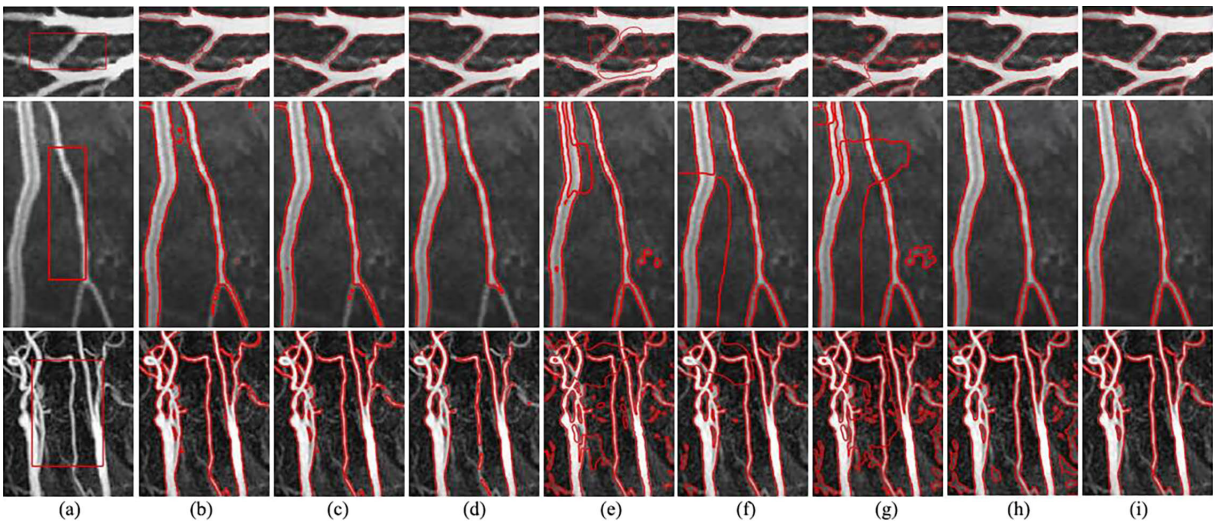

FIGURE 9. Segmentation results of vessel images with complex background. (a) Original images with initial contours. (b)-(i) Results of CV, FEBAC, FRAGL, EWF, LBF, LIF, GLSEPF and our model. Row 1: pulmonary vessel (ultrasonic imaging). Row 2: abdominal vessel (computed tomography). Row 3: carotid vessel (magnetic resonance angiography).

based models can deal with images with intensity inhomogeneity, but they are sensitive to the position of the initial contour. On the other hand, introducing global image information into ACM is necessary to improve the robustness of the method to initial contour. Although, both GLSEPF and our model are a hybrid model based on global and local information, our model performs better. The main reason is that the proposed adaptive fuzzy force greatly avoids the proposed model trapping into local minimum.

2) SEGMENTATION OF BIMODAL AND INHOMOGENEOUS IMAGES

In Fig. 8, two bimodal images and four inhomogeneous images are used to visually evaluate the performance of the proposed model and the compared methods. Fig. 8(a) shows the original images with the initial contours. Figs. 8(b)-(i) are the segmentation results of the CV, EWF, FEBAC, FRAGL, LBF, LIF, GLSEPF and the propose model, respectively. From rows 1 and 2, we can observe that all methods can work

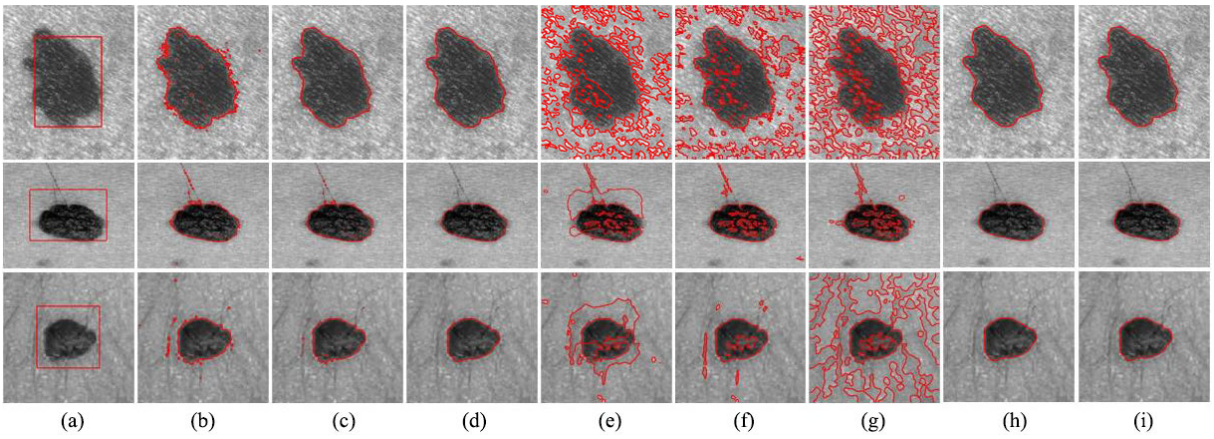

FIGURE 10. Segmentation results of skin lesion images. (a) Original images with initial contours. (b)-(i) Results of CV, FEBAC, FRAGL, EWF, LBF, LIF, GLSEPF and our model.

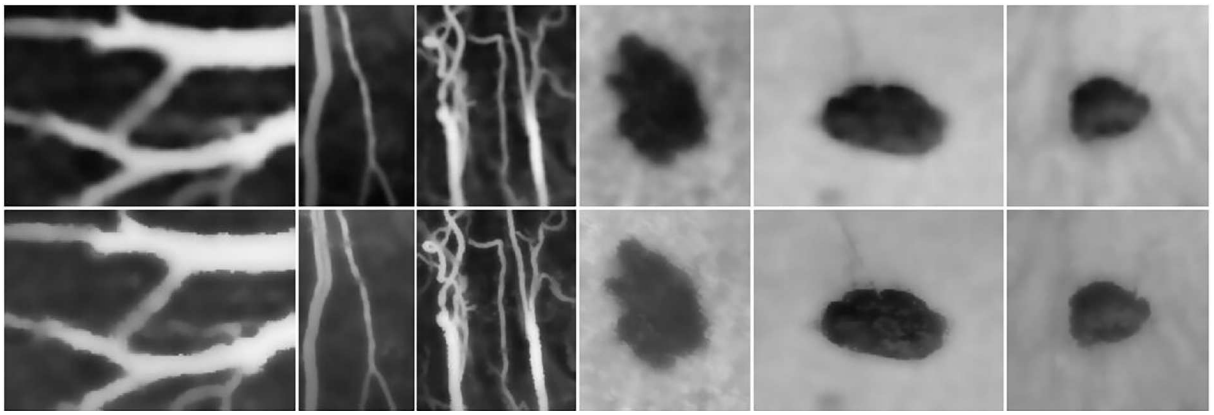

FIGURE 11. Local fitted images of images in Figs. 9 and 10. Row 1: the proposed I^{FLFI}. Row 2: I^{LFI} proposed in the LIF model.

well on bimodal images. But CV and FEBAC cannot efficiently segment inhomogeneous images as shown in columns 2 and 3 due to only using the global mean of intensities. Even though FRAGL is the local-region based model and has better performance in row 5, it cannot get desirable segmentation results in rows 3, 4 and 6, the reason may be that the weight used to compute the local means cannot efficiently capture the local information of images. On the contrary, EWF, LIF, LBF, GLSEPF and the proposed model obtain satisfactory segmentation results for these inhomogeneous images. This demonstrates that efficiently extracting local information of images plays a vital role in segmenting images with intensity inhomogeneity.

3) SEGMENTATION OF MEDICAL IMAGES

In computer-aid medical image analysis, correctly extracting the required boundaries of the target objects is very important for the doctor's diagnosis. For example, the boundaries of skin lesion can be utilized to asses the risk of melanoma. In order to further test the ability to segment images with complex background, we conduct the following experiments shown in Figs. 9 and 10. Fig. 9 shows the vessel segmentation of different modalities: pulmonary vessel (ultrasonic imaging), abdominal vessel (computed tomography) and carotid vessel (magnetic resonance angiography).

TABLE 1. Segmentation accuracy of our method compared with the state-of-the-art methods shown in Figs. 8-10.

Image	CV	FEBAC	FRAGL	EWF	LBF	LIF	GLSEPF	Ours
Row 1 Fig. 8	0.9930	0.9911	0.9871	0.9524	0.9958	0.9948	0.9935	**0.9963**
Row 2 Fig. 8	1.0000	1.0000	0.9992	0.9996	1.0000	1.0000	1.0000	**1.0000**
Row 3 Fig. 8	0.5544	0.5542	0.5616	0.9768	0.9720	0.9735	0.9751	**0.9780**
Row 4 Fig. 8	0.5717	0.5785	0.5846	0.9772	0.9793	0.9659	0.9795	**0.9804**
Row 5 Fig. 8	0.2996	0.3186	0.8002	0.8685	0.8998	0.9001	0.8654	**0.9113**
Row 6 Fig. 8	0.2992	0.2984	0.3012	0.9670	0.9659	0.9663	0.9656	**0.9673**
Row 1 Fig. 9	0.9254	0.8887	0.9435	0.7047	0.6960	0.6827	0.9555	**0.9615**
Row 2 Fig. 9	0.9026	0.8305	0.8680	0.7726	0.8083	0.7921	0.9541	**0.9579**
Row 3 Fig. 9	0.9045	0.8222	0.7710	0.6241	0.6324	0.6216	0.8192	**0.8358**
Row 1 Fig. 10	0.9590	0.9553	0.9661	0.6360	0.7097	0.6023	0.9700	**0.9705**
Row 2 Fig. 10	0.9636	0.9437	0.9547	0.7631	0.8725	0.8834	0.9726	**0.9732**
Row 3 Fig. 10	0.9673	0.9583	0.9639	0.6903	0.8525	0.6218	0.9756	**0.9772**

Segmentation results of three skin lesion images corrupted by noise are shown in Fig. 10. From these segmentation results, it can be seen that the proposed model works well on these images. GLSEPF obtains desirable results of skin lesion images, but fails to extract the boundary of the carotid vessel image as shown in row 3 of Fig. 9. However, the other compared models cannot get satisfactory segmentation results. However, CV, FEBAC and FRAGL are better than EWF, LBF and LIF. This just verifies what we mentioned earlier that global-based models are less likely to fall into local minimum than local-based models. But the proposed model avoids this drawback by integrating local fuzzy statistical

FIGURE 12. The final stopping positions of the zero level set for natural image from MSRA-B database using different models. Row 1: The original images with initial contours marked by blue line. Rows 2-9: Results of CV, FEBAC, FRAGL, EWF, LBF, LIF, GLSEPF and our model.

information and global based adaptive force into the energy functional, which makes the proposed more effective to deal with intensity inhomogeneity and more robust to images with complex background. Fig. 11 shows the fuzzy local fitted images corresponding to images in Figs. 9 and 10. We can find that the proposed I^{FLFI} is more capable of effectively highlighting the desirable objects than I^{LFI} proposed in [13], which makes the proposed model less susceptible to complex backgrounds in image segmentation.

4) QUANTITATIVE EVALUATION

In this section, Dice Similarity Coefficient (DSC) [18] is used to quantitatively evaluate the accuracy of the proposed model, and the DSC is given by:

$$DSC(G,T) = \frac{2 \times |G \bigcap T|}{|G| + |T|} \tag{37}$$

where $|G|$, $|T|$ and $|G \bigcap T|$ denote the pixel number of the regions G, T and their union area, respectively. G is the

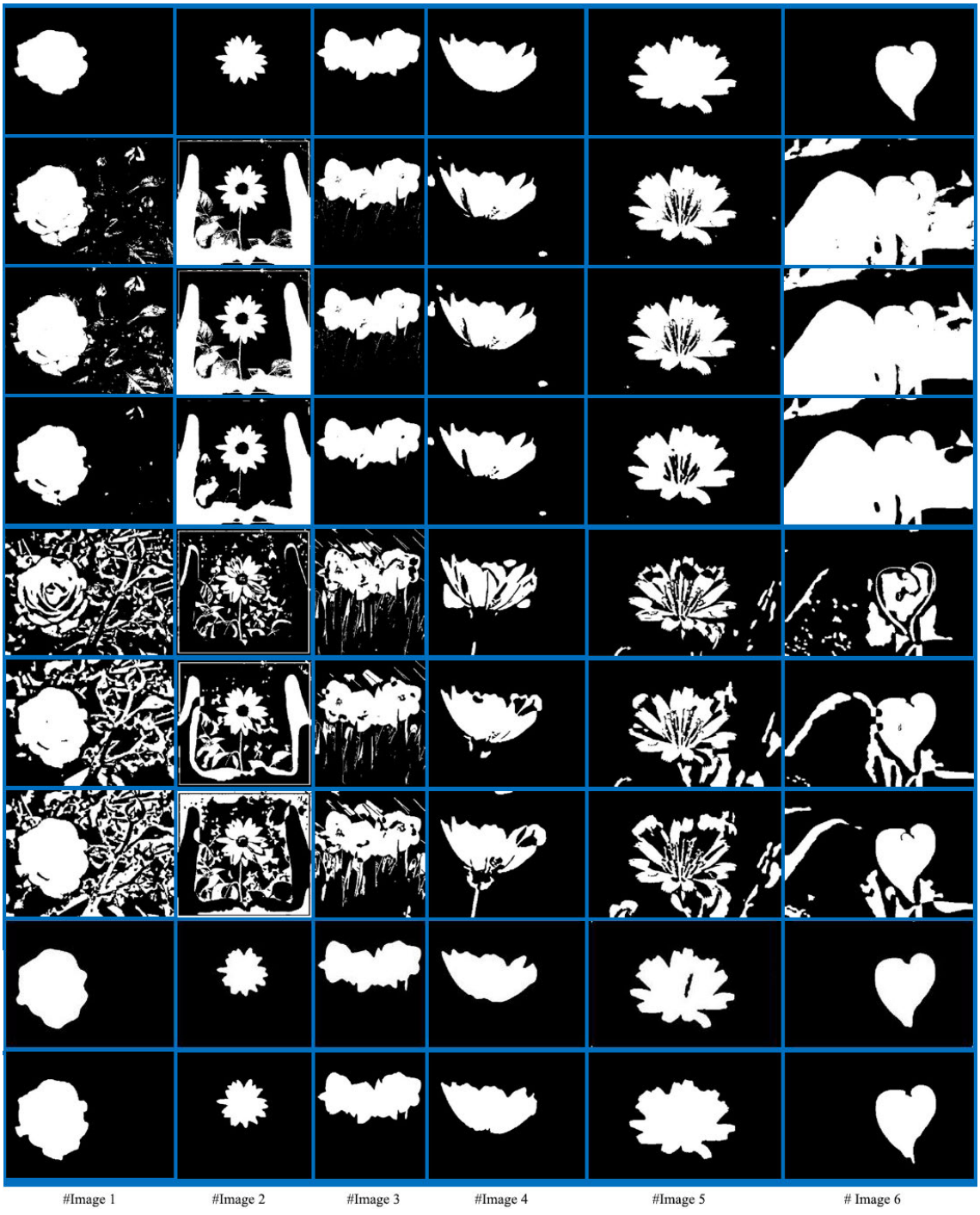

FIGURE 13. Segmentation results in Fig. 12 using different models. Row 1: Ground truth. Rows 2-9: CV, FEBAC, FRAGL, EWF, LBF, LIF, GLSEPF and our model.

ground-truth segmentation. T is the segmentation results of the corresponding methods. Obviously, the value of DSC varies between 0 and 1, and the closer DSC value is to 1, the better the segmentation is. The DSC of images in Figs. 8-10 are listed in Table 1, in which the proposed model obtains comparable results. In addition, we can find that the accuracy of global and local based models (GLSEPF and our model) is better than that of global or local based models.

In addition, natural images from MSRA-B are used to further evaluate the proposed model. It is worth noting that the used color images are first transformed into a gray image before segmentation according to the formula: $I = 0.299 * I_R + 0.587 * I_G + 0.114 * I_B$, here I_R, I_G and I_B present the pixel values corresponding to the R, G and B channels, respectively. From Figs. 12 and 13, we can find that the proposed model and GLSEPF can exactly extract the desirable boundaries of the objects in the tested images, which include

TABLE 2. Comparison of the proposed model with the CV, FEBAC, FRAGL, EWF, LBF, LIF and GLSEPF based on DSC for nature images in Fig. 10.

Image	CV	FEBAC	FRAGL	EWF	LBF	LIF	GLSEPF	Ours
Image 1	0.9071	0.8436	0.9687	0.5141	0.6002	0.5510	0.9845	**0.9913**
Image 2	0.2790	0.2734	0.2989	0.4515	0.3453	0.3074	0.9787	**0.9881**
Image 3	0.9797	0.9798	0.9843	0.7827	0.8480	0.7385	0.9879	**0.9905**
Image 4	0.9268	0.9272	0.9301	0.8074	0.8837	0.8352	0.9565	**0.9571**
Image 5	0.9412	0.9419	0.9364	0.7343	0.6910	0.5324	0.9787	**0.9874**
Image 6	0.3363	0.3174	0.3308	0.5509	0.6861	0.6845	0.9825	**0.9869**

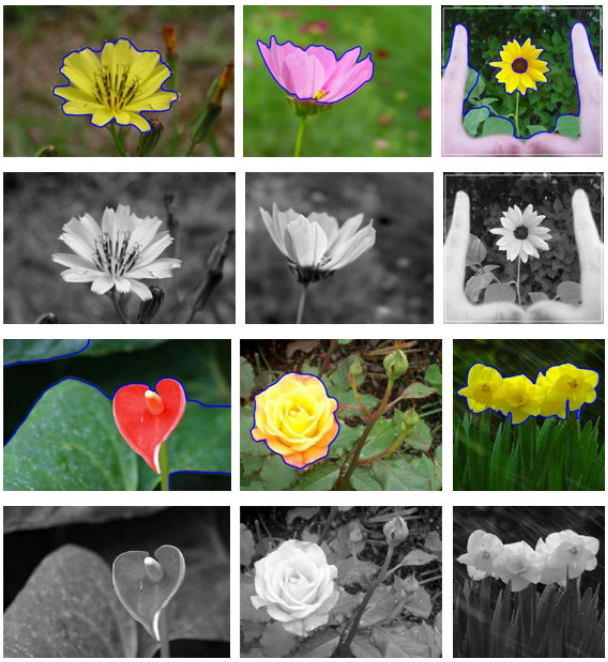

FIGURE 14. Rows 1 and 3: Segmentation of the images shown in Fig. 12 and the pseudo LSF are initialized as a constant function($u(x) = 0.5, x \in \Omega$). Rows 2 and 4: The corresponding gray images.

severe intensity inhomogeneity. By contrast, other compared models fail to segment these images. To clearly compare the performance of all methods, the segmentation accuracy of images shown in Fig. 12 in terms of DSC are listed in Table 2. Compared with other models, the proposed model and GLSEPF obtain more satisfactory results. But the segmentation accuracy of the proposed model is slightly higher than that of GLSEPF.

V. DISCUSSION

A. INITIALIZATION OF PSEUDO LEVEL SET FUNCTION

As we mentioned earlier that the pseudo LSF of the proposed model can be initialized as a constant function (e.g. $u(x) = 0.5, x \in \Omega$), and the effectiveness of this strategy has been confirmed in some experiments. But this does not mean it can work well on all types of images. An example is shown in Fig. 14. It can be observed that the developed method can exactly extract the boundaries of the target objects with the position of the initial contour shown in row 1 of Fig. 12. However, when the pseudo LSF is initialized as a constant function, the proposed model cannot successfully segment all images as shown in Fig. 14. From the corresponding gray images, we can get the following inference. If the target object

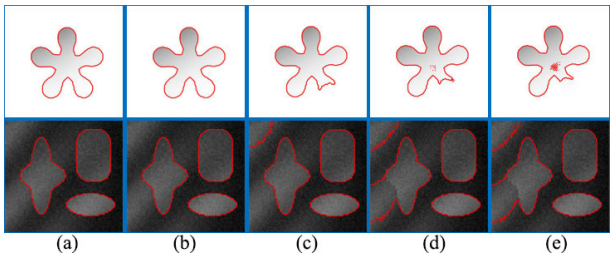

FIGURE 15. Segmentation results based on different γ. (a) $\gamma = 0.05$. (b) γ=0.1. (c) $\gamma = 0.2$. (d) $\gamma = 0.3$. (e) $\gamma = 0.4$.

is darker or brighter than the background region, the proposed model can obtain desirable segmentation result. On contrary, if a large part of the target object is similar to the background region, the proposed model will not work well and even gets wrong segmentation results.

B. INFLUENCE OF THE PARAMETER γ

The proposed adaptive force, which is constructed by using global information of image, plays a key role in rejecting the shortcomings suffered by local region-based models. In the following experiment, we show the effect of parameter γ on the proposed model. Fig. 15 shows the segmentation results under the parameter γ, which is set to be 0.05, 0.1, 0.2, 0.3 and 0.4, respectively. It can be seen that two images are corrupted by intensity inhomogeneity and the proposed model obtain the desirable results by setting $\gamma = 0.05$ and $\gamma = 0.01$. However, the objects cannot be segmented successfully in other cases. In fact, the parameter γ should be set according to the image. In general, If the image contains severe intensity inhomogeneity, a small value γ should be chosen, and vice versa. Fortunately, $\gamma = 0.05$ works well on all tested images in this paper.

VI. CONCLUSION

In this work, a fuzzy local-region based ACM is presented to segment images with intensity inhomogeneity. The proposed model has some advantages over several famous models due to the following reason. Firstly, the defined fuzzy local fitted images effectively reduces a large number of undesired background information and fits the target objects well. Secondly, the proposed weighting method based on the edge indicator, which is defined on fractional-order diffusion, provides underlying boundaries of the target objects and helps the proposed model to segmentation images with weak boundaries. Thirdly, the local FSPF makes the evolving curve automatically move toward the boundaries of the target objects. Finally, the global FSPF prevents the proposed model from falling into local minimum and allows our model to have more flexible initialization method. Moreover, the level set evolution can start with a constant function. Experimental results demonstrate that the desirable performance of our model for segmenting both synthetic and real images with intensity inhomogeneity in terms of accuracy. But the proposed model cannot work well on the images when a large part of the target object is very similar to the background region.

APPENDIX A. PROOF OF THEOREM A

Proof: In ω, we get

$$\begin{aligned} a - u_1(x)c_1 - u_2(x)c_2 &= u_1(x)(a - c_1) + u_2(x)(a - c_2) \\ &= \sum_{i=1}^{2} u_i(x)\frac{\int_\Omega [u_i(x)]^m (a - I(x))dx}{\int_\Omega [u_i(x)]^m dx} \\ &= \sum_{i=1}^{2} u_i(x)\frac{\int_{\Omega\setminus\omega} [u_i(x)]^m (a - b)dx}{\int_\Omega [u_i(x)]^m dx} \\ &= (a-b)\sum_{i=1}^{2} u_i(x)\frac{\int_{\Omega\setminus\omega} [u_i(x)]^m dx}{\int_\Omega [u_i(x)]^m dx} \end{aligned} \tag{A.1}$$

But also the following facts

$$\sum_{i=1}^{2} u_i(x)\frac{\int_{\Omega\setminus\omega} [u_i(x)]^m dx}{\int_\Omega [u_i(x)]^m dx} > 0 \tag{A.2}$$

Therefore

$$sign(a - u_1(x)c_1 - u_2(x)c_2) = +sign(a - b) \tag{A.3}$$

Similarly, In $\Omega\setminus\omega$

$$sign(b - u_1(x)c_1 - u_2(x)c_2) = -sign(a - b) \tag{A.4}$$

From (A.3) and (A.4), we get

$$sign(spf_G(I(x)) = \begin{cases} +sign(a-b), & in\ \omega \\ -sign(s-b), & in\ \Omega \setminus \omega \end{cases} \tag{A.5}$$

This completes the proof.

APPENDIX B. PROOF OF THEOREM B

Proof: Let $Q = \int_\Omega K_\sigma(x-y)[u_1(y)]^m dy$, $q = \int_\omega K_\sigma(x-y)[u_1(y)]^m dy$, $P = \int_\Omega K_\sigma(x-y)[u_2(y)]^m dy$, $p = \int_\omega K_\sigma(x-y)[u_2(y)]^m dy$. Thus, by (19), we have

$$\begin{aligned} &m_1(x) \\ &= \frac{\int_\Omega K_\sigma(x-y)I(y)[u_1(y)]^m dy}{\int_\Omega K_\sigma(x-y)[u_1(y)]^m dy} \\ &= \frac{a\int_\omega K_\sigma(x-y)[u_1(y)]^m dy + b\int_{\Omega\setminus\omega} K_\sigma(x-y)[u_1(y)]^m dy}{\int_\Omega K_\sigma(x-y)[u_1(y)]^m dy} \\ &= \frac{aq + b(Q-q)}{Q} = \frac{(a-b)q + bQ}{Q} \end{aligned} \tag{B.1}$$

$$\begin{aligned} &m_2(x) \\ &= \frac{\int_\Omega K_\sigma(x-y)I(y)[u_2(y)]^m dy}{\int_\Omega K_\sigma(x-y)[u_2(y)]^m dy} \\ &= \frac{a\int_\omega K_\sigma(x-y)[u_2(y)]^m dy + b\int_{\Omega\setminus\omega} K_\sigma(x-y)[u_2(y)]^m dy}{\int_\Omega K_\sigma(x-y)[u_2(y)]^m dy} \\ &= \frac{ap + b(P-p)}{P} = \frac{(a-b)p + bP}{P} \end{aligned} \tag{B.2}$$

Therefore, in ω, we get

$$\begin{aligned} &a - m_1(x)u_1(x) - m_2(x)u_2(x) \\ &= (a-b)\left[\frac{Q-q}{Q}u_1(x) + \frac{P-p}{P}u_2(x)\right] \\ &= (a-b)\left(1 - \left[\frac{q}{Q}u_1(x) + \frac{p}{P}u_2(x)\right]\right) \end{aligned} \tag{B.3}$$

in $\Omega\setminus\omega$, we have

$$\begin{aligned} &b - m_1(x)u_1(x) - m_2(x)u_2(x) \\ &= -(a-b)\left(\frac{q}{Q}u_1(x) + \frac{p}{P}u_2(x)\right) \end{aligned} \tag{B.4}$$

Since $u_1(x), u_2(x) \in [0, 1]$ and $u_1(x) + u_2(x) = 1$, therefore

$$0 < \frac{q}{Q}u_1(x) + \frac{p}{P}u_2(x) = \frac{p}{P} < 1 \tag{B.5}$$

Hence

$$sign(a - \sum_{i=1}^{2} u_i(x)m_i(x)) = +sign(a-b) \tag{B.6}$$

Similarly, In $\Omega\setminus\omega$

$$sign(b - \sum_{i=1}^{2} u_i(x)m_i(x)) = -sign(a-b) \tag{B.7}$$

From (B.6) and (B.7), we get

$$sign(spf_L(I(x)) = \begin{cases} +sign(a-b), & in\ \omega \\ -sign(s-b), & in\ \Omega \setminus \omega \end{cases} \tag{B.8}$$

This completes the proof.

REFERENCES

[1] D. Cremers, M. Rousson, and R. Deriche, "A review of statistical approaches to level set segmentation: Integrating color, texture, motion and shape," *Int. J. Comput. Vis.*, vol. 72, no. 2, pp. 195–215, Apr. 2007.
[2] M. Kass, A. Witkin, and D. Terzopoulos, "Snakes: Active contour models," *Int. J. Comput. Vis.*, vol. 1, no. 4, pp. 321–331, Jan. 1988.
[3] R. Malladi, J. A. Sethian, and B. C. Vemuri, "Shape modeling with front propagation: A level set approach," *IEEE Trans. Pattern Anal. Mach. Intell.*, vol. 17, no. 2, pp. 158–175, Feb. 1995.
[4] V. Estellers, D. Zosso, R. Lai, S. Osher, J. Thiran, and X. Bresson, "Efficient algorithm for level set method preserving distance function," *IEEE Trans. Image Process.*, vol. 21, no. 12, pp. 4722–4734, Dec. 2012.
[5] V. Caselles, F. Catté, T. Coll, and F. Dibos, "A geometric model for active contours in image processing," *Numerische Math.*, vol. 66, no. 1, pp. 1–31, Dec. 1993.
[6] V. Caselles, R. Kimmel, and G. Sapiro, "Geodesic active contours," *Int. J. Comput. Vis.*, vol. 22, no. 1, pp. 61–79, Feb. 1997.
[7] A. Khadidos, V. Sanchez, and C.-T. Li, "Weighted level set evolution based on local edge features for medical image segmentation," *IEEE Trans. Image Process.*, vol. 26, no. 4, pp. 1979–1991, Apr. 2017.
[8] A. Vasilevskiy and K. Siddiqi, "Flux maximizing geometric flows," *IEEE Trans. Pattern Anal. Mach. Intell.*, vol. 24, no. 12, pp. 1565–1578, Dec. 2002.
[9] C. Liu, W. Liu, and W. Xing, "An improved edge-based level set method combining local regional fitting information for noisy image segmentation," *Signal Process.*, vol. 130, pp. 12–21, Jan. 2017.
[10] T. F. Chan and L. A. Vese, "Active contours without edges," *IEEE Trans. Image Process.*, vol. 10, no. 2, pp. 266–277, Feb. 2001.
[11] C. Li, C.-Y. Kao, J. C. Gore, and Z. Ding, "Implicit active contours driven by local binary fitting energy," in *Proc. IEEE Conf. Comput. Vis. Pattern Recognit.*, Jun. 2007, pp. 1–7.
[12] C. Li, C.-Y. Kao, J. C. Gore, and Z. Ding, "Minimization of region-scalable fitting energy for image segmentation," *IEEE Trans. Image Process.*, vol. 17, no. 10, pp. 1940–1949, Oct. 2008.
[13] K. Zhang, H. Song, and L. Zhang, "Active contours driven by local image fitting energy," *Pattern Recognit.*, vol. 43, no. 4, pp. 1199–1206, Apr. 2010.
[14] C. He, Y. Wang, and Q. Chen, "Active contours driven by weighted region-scalable fitting energy based on local entropy," *Signal Process.*, vol. 92, no. 2, pp. 587–600, Feb. 2012.
[15] L. Wang, Y. Chang, H. Wang, Z. Wu, J. Pu, and X. Yang, "An active contour model based on local fitted images for image segmentation," *Inf. Sci.*, vols. 418–419, pp. 61–73, Dec. 2017.

[16] L. Wang, L. Zhang, X. Yang, P. Yi, and H. Chen, "Level set based segmentation using local fitted images and inhomogeneity entropy," *Signal Process.*, vol. 167, Feb. 2020, Art. no. 107297.
[17] K. Zhang, L. Zhang, K.-M. Lam, and D. Zhang, "A level set approach to image segmentation with intensity inhomogeneity," *IEEE Trans. Cybern.*, vol. 46, no. 2, pp. 546–557, Feb. 2016.
[18] K. Zhang, L. Zhang, H. Song, and W. Zhou, "Active contours with selective local or global segmentation: A new formulation and level set method," *Image Vis. Comput.*, vol. 28, no. 4, pp. 668–676, Apr. 2010.
[19] X. Shan, X. Gong, Y. Ren, and A. K. Nandi, "Image segmentation using an active contour model based on the difference between local intensity averages and actual image intensities," *IEEE Access*, vol. 8, pp. 43200–43214, 2020.
[20] L. Fang, T. Qiu, H. Zhao, and F. Lv, "A hybrid active contour model based on global and local information for medical image segmentation," *Multidimensional Syst. Signal Process.*, vol. 30, no. 2, pp. 689–703, Apr. 2019.
[21] F. Akram, M. A. Garcia, and D. Puig, "Active contours driven by local and global fitted image models for image segmentation robust to intensity inhomogeneity," *PLoS ONE*, vol. 12, no. 4, Apr. 2017, Art. no. e0174813.
[22] M. M. Abdelsamea and G. Gnecco, "Robust local–global SOM-based ACM," *Electron. Lett.*, vol. 51, no. 2, pp. 142–143, Jan. 2015.
[23] L. Fang, T. Qiu, Y. Liu, and C. Chen, "Active contour model driven by global and local intensity information for ultrasound image segmentation," *Comput. Math. Appl.*, vol. 75, no. 12, pp. 4286–4299, Jun. 2018.
[24] H. Wang, T.-Z. Huang, Z. Xu, and Y. Wang, "A two-stage image segmentation via global and local region active contours," *Neurocomputing*, vol. 205, pp. 130–140, Sep. 2016.
[25] H. Ali, N. Badshah, K. Chen, and G. A. Khan, "A variational model with hybrid images data fitting energies for segmentation of images with intensity inhomogeneity," *Pattern Recognit.*, vol. 51, pp. 27–42, Mar. 2016.
[26] B. Han and Y. Wu, "Active contours driven by global and local weighted signed pressure force for image segmentation," *Pattern Recognit.*, vol. 88, pp. 715–728, Apr. 2019.
[27] J. Fang, H. Liu, L. Zhang, J. Liu, and H. Liu, "Active contour driven by weighted hybrid signed pressure force for image segmentation," *IEEE Access*, vol. 7, pp. 97492–97504, 2019.
[28] H. Liu, J. Fang, Z. Zhang, and Y. Lin, "A novel active contour model guided by global and local signed energy-based pressure force," *IEEE Access*, vol. 8, pp. 59412–59426, 2020.
[29] C. Li, C. Xu, C. Gui, and M. D. Fox, "Distance regularized level set evolution and its application to image segmentation," *IEEE Trans. Image Process.*, vol. 19, no. 12, pp. 3243–3254, Dec. 2010.
[30] L. Wang and C. Pan, "Robust level set image segmentation via a local correntropy-based K-means clustering," *Pattern Recognit.*, vol. 47, no. 5, pp. 1917–1925, May 2014.
[31] S. Krinidis and V. Chatzis, "Fuzzy energy-based active contours," *IEEE Trans.s Image Process.*, vol. 18, no. 12, pp. 2747–2755, Dec. 2009.
[32] S. Soomro, A. Munir, and K. N. Choi, "Fuzzy c-means clustering based active contour model driven by edge scaled region information," *Expert Syst. Appl.*, vol. 120, pp. 387–396, Apr. 2019.
[33] R. Jin and G. Weng, "A robust active contour model driven by fuzzy c-means energy for fast image segmentation," *Digit. Signal Process.*, vol. 90, pp. 100–109, Jul. 2019.
[34] S. Jayanthi, H. Ranganathan, and M. Palanivelan, "Segmenting brain tumour regions with fuzzy integrated active contours," *IETE J. Res.*, to be published, doi: 10.1080/03772063.2019.1615007.
[35] Z. Zhang and J. Song, "An adaptive fuzzy level set model with local spatial information for medical image segmentation and bias correction," *IEEE Access*, vol. 7, pp. 27332–27338, 2019.
[36] X. Wang, Z. Jiang, W. Li, R. Zarei, G. Huang, A. Ulhaq, X. Yin, B. Zhang, P. Shi, M. Guo, and J. He, "Active contours with local and global energy based-on fuzzy clustering and maximum a posterior probability for retinal vessel detection," *Concurrency Comput., Pract. Exper.*, vol. 32, no. 7, p. e5599, Apr. 2020.
[37] Y. Wu, W. Ma, M. Gong, H. Li, and L. Jiao, "Novel fuzzy active contour model with kernel metric for image segmentation," *Appl. Soft Comput.*, vol. 34, pp. 301–311, Sep. 2015.
[38] W. Sun, E. Dong, and H. Qiao, "A fuzzy energy-based active contour model with adaptive contrast constraint for local segmentation," *Signal, Image Video Process.*, vol. 12, no. 1, pp. 91–98, Jan. 2018.
[39] V.-T. Pham, T.-T. Tran, K.-K. Shyu, C. Lin, P.-C. Wang, and M.-T. Lo, "Shape collaborative representation with fuzzy energy based active contour model," *Eng. Appl. Artif. Intell.*, vol. 56, pp. 60–74, Nov. 2016.
[40] H. Lv, Z. Wang, S. Fu, C. Zhang, L. Zhai, and X. Liu, "A robust active contour segmentation based on fractional-order differentiation and fuzzy energy," *IEEE Access*, vol. 5, pp. 7753–7761, 2017.
[41] H. Lv, S. Fu, C. Zhang, and X. Liu, "Non-local weighted fuzzy energy-based active contour model with level set evolution starting with a constant function," *IET Image Process.*, vol. 13, no. 7, pp. 1115–1123, May 2019.
[42] M. Gong, D. Tian, L. Su, and L. Jiao, "An efficient bi-convex fuzzy variational image segmentation method," *Inf. Sci.*, vol. 293, pp. 351–369, Feb. 2015.
[43] S. Luo, K. Sarabandi, L. Tong, and S. Guo, "Unsupervised multiregion partitioning of fully polarimetric SAR images with advanced fuzzy active contours," *IEEE Trans. Geosci. Remote Sens.*, vol. 58, no. 2, pp. 1475–1486, Feb. 2020.
[44] A. Ahmad, N. Badshah, and H. Ali, "A fuzzy variational model for segmentation of images having intensity inhomogeneity and slight texture," *Soft Comput.*, vol. 24, pp. 15491–15506, Apr. 2020.
[45] A. Mondal, S. Ghosh, and A. Ghosh, "Robust global and local fuzzy energy based active contour for image segmentation," *Appl. Soft Comput.*, vol. 47, pp. 191–215, Oct. 2016.
[46] K.-K. Shyu, V.-T. Pham, T.-T. Tran, and P.-L. Lee, "Global and local fuzzy energy-based active contours for image segmentation," *Nonlinear Dyn.*, vol. 67, no. 2, pp. 1559–1578, Jan. 2012.
[47] T.-T. Tran, V.-T. Pham, and K.-K. Shyu, "Image segmentation using fuzzy energy-based active contour with shape prior," *J. Vis. Commun. Image Represent.*, vol. 25, no. 7, pp. 1732–1745, Oct. 2014.
[48] J. Fang, H. Liu, L. Zhang, J. Liu, and H. Liu, "Fuzzy region-based active contours driven by weighting global and local fitting energy," *IEEE Access*, vol. 7, pp. 184518–184536, 2019.
[49] A. Mondal, S. Ghosh, and A. Ghosh, "Partially camouflaged object tracking using modified probabilistic neural network and fuzzy energy based active contour," *Int. J. Comput. Vis.*, vol. 122, no. 1, pp. 116–148, Mar. 2017.
[50] A. Mondal, "Fuzzy energy based active contour model for multi-region image segmentation," *Multimedia Tools Appl.*, vol. 79, nos. 1–2, pp. 1535–1554, Jan. 2020.
[51] K.-K. Shyu, T.-T. Tran, V.-T. Pham, P.-L. Lee, and L.-J. Shang, "Fuzzy distribution fitting energy-based active contours for image segmentation," *Nonlinear Dyn.*, vol. 69, nos. 1–2, pp. 295–312, Jul. 2012.
[52] T.-T. Tran, V.-T. Pham, and K.-K. Shyu, "Zernike moment and local distribution fitting fuzzy energy-based active contours for image segmentation," *Signal, Image Video Process.*, vol. 8, no. 1, pp. 11–25, Jan. 2014.
[53] M. M. Abdelsamea, A. Pitiot, R. B. Grineviciute, J. Besusparis, A. Laurinavicius, and M. Ilyas, "A cascade-learning approach for automated segmentation of tumour epithelium in colorectal cancer," *Expert Syst. Appl.*, vol. 118, pp. 539–552, Mar. 2019.
[54] W. Kim and C. Kim, "Active contours driven by the salient edge energy model," *IEEE Trans. Image Process.*, vol. 22, no. 4, pp. 1667–1673, Apr. 2013.
[55] X. Yin and S. Zhou, "Image structure-preserving denoising based on difference curvature driven fractional nonlinear diffusion," *Math. Problems Eng.*, vol. 2015, Apr. 2015, Art. no. 930984.
[56] J. Bai and X.-C. Feng, "Fractional-order anisotropic diffusion for image denoising," *IEEE Trans. Image Process.*, vol. 16, no. 10, pp. 2492–2502, Oct. 2007.
[57] Q. Chen, P. Montesinos, Q. S. Sun, P. A. Heng, and D. S. Xia, "Adaptive total variation denoising based on difference curvature," *Image Vis. Comput.*, vol. 28, no. 3, pp. 298–306, Mar. 2010.

HONGLI LV received the B.S. degree from the School of Mathematics and Statistics, Henan University, Kaifeng, China, in 2007, the M.S. degree from the College of Mathematics and Information Science, Wenzhou University, Wenzhou, China, in 2015, and the Ph.D. degree in computational mathematics from Shandong University, in 2018. He is currently a Lecturer with the School of Information Technology, Shangqiu Normal University. He is also a Research Associate with the College of Big Data and Software Engineering, Zhejiang Wanli University. His research interests include medical image processing and computer vision, especially image denoising and image segmentation.

FANGJIAN ZHANG received the B.S. degree from Shangqiu Normal University, Shangqiu, China, in 2006. He is currently a Senior Research Assistant with the School of Information Technology, Shangqiu Normal University. His research interests include image processing, multimedia processing technology, and intelligence computation.

RENFANG WANG received the Ph.D. degree from the State Key Laboratory of CAD and CG, Zhejiang University. He is currently a Professor with the College of Big Data and Software Engineering, Zhejiang Wanli University. He holds the third level of 151 Talent Project, Zhejiang, and the second level of Leading Talents, Ningbo. His research interests include computer graphics, image processing, and multimedia processing technology.